Computers and Concrete, *Vol. 23, No. 1 (2019) 11-23*
DOI: https://doi.org/10.12989/cac.2019.23.1.011

Validation of a non-linear hinge model for tensile behavior of UHPFRC using a Finite Element Model

Eduardo J. Mezquida-Alcaraz*, Juan Navarro-Gregori[a], Juan Ángel López[b] and Pedro Serna-Ros[c]

Instituto de Ciencia y Tecnología del Hormigón (ICITECH), Universitat Politècnica de València, Camino de Vera s/n, 46022, València, Spain

(Received August 15, 2018, Revised January 5, 2019, Accepted January 15, 2019)

Abstract. Nowadays, the characterization of Ultra-High Performance Fiber-Reinforced Concrete (UHPFRC) tensile behavior still remains a challenge for researchers. For this purpose, a simplified closed-form non-linear hinge model based on the Third Point Bending Test (ThirdPBT) was developed by the authors. This model has been used as the basis of a simplified inverse analysis methodology to derive the tensile material properties from load-deflection response obtained from ThirdPBT experimental tests. In this paper, a non-linear finite element model (FEM) is presented with the objective of validate the closed-form non-linear hinge model. The state determination of the closed-form model is straightforward, which facilitates further inverse analysis methodologies to derive the tensile properties of UHPFRC. The accuracy of the closed-form non-linear hinge model is validated by a robust non-linear FEM analysis and a set of 15 Third-Point Bending tests with variable depths and a constant slenderness ratio of 4.5. The numerical validation shows excellent results in terms of load-deflection response, bending curvatures and average longitudinal strains when resorting to the discrete crack approach.

Keywords: finite element model; numerical validation; ultra-high performance fiber-reinforced concrete; closed-form non-linear hinge model; third point bending test; smeared cracking approach; discrete cracking approach

1. Introduction

Ultra-High Performance Fiber-Reinforced Concrete (UHPFRC) can be defined as a hydraulic cement-based composite material that combines three technologies in concrete: (i) high characteristic compressive strength of more than 130 MPa; (ii) ductile behavior under tension due to the presence of fibers, which can or cannot provide a pseudo strain-hardening stress-strain response accompanied by multiple cracking depending on fiber volumetric fraction, the fiber aspect ratio, and also the fiber distribution inside the structural element; (iii) a special selection of fine and ultrafine aggregates that provides dense particle packing, high durability and a certain degree of flowability (López 2017). In this way, the UHPFRC that manifests a strain-hardening response can be considered a special type of high-performance fiber-reinforced cement composite (HPFRCC) (López *et al*. 2015a). Accordingly, HPFRCC can be characterized as all the concrete that exhibits a strain hardening tensile stress-strain response accompanied by multiple cracking and relatively large energy absorption capacity. Consequently, a standard mechanical characterization test must provide the tool to obtain strain hardening behavior, commonly described as a stress-strain relationship, and softening behavior also has to be provided. As macro-crack formation is a discrete phenomenon, this behavior may be based on a fracture mechanics approach and be described using a similar stress-crack opening relationship to that proposed in (Casanova and Rossi 1996, Olesen 2001, Ostergaard *et al*. 2005, Pedersen 1996, Stang and Olesen 1998).

Nowadays, the characterization of UHPFRC tensile behavior is still a challenge, and no agreement on the standard test set up, advisability of notch, or even specimen shape and size, has yet been reached. As notched three-point bending tests do not make the characterization of strain hardening behavior possible, and uniaxial tensile tests are difficult to perform and lead to the development of suitable easy-to-conduct tests (Graybeal and Baby 2013, Kanakubo 2006, Ostergaard *et al*. 2005, Qian and Li 2007, Wille *et al*. 2014), four-point bending tests (4PBTs) arise as the best ones to obtain both behaviors. However, 4PBTs require the use of an inverse analysis methodology to derive the tensile properties from the results obtained from it. Different inverse analysis methods have already been developed to obtain the parameters that define the UHPFRC behavior in tension from 4PBT (Baby *et al*. 2012, 2013, Gröger *et al*. 2012, López *et al*. 2015a, Maalej and Li 1994, Ostergaard *et al*. 2005, Qian and Li 2007, Rigaud *et al*. 2012, Soranakom and Mobasher 2007).

To determine the validity and accuracy of inverse analysis methods, it is important to develop numerical models. In the literature, it is possible to find numerical

*Corresponding author, Ph.D. Student
E-mail: edmezal@alumni.upv.es
[a]Professor
E-mail: juanagre@cst.upv.es
[b]Ph.D.
E-mail: jualoma7@gmail.com
[c]Professor
E-mail: pserna@cst.upv.es

http://www.techno-press.org/?journal=cac&subpage=8 ISSN: 1598-8198 (Print), 1598-818X (Online)

models for UHPFRC using finite element modeling (FEM). Frequently, the concrete material model available in finite element packages is validated with the limited number of tests conducted on material and structural members (Singh *et al*. 2017). The material characteristics and the calibrations for the numerical model can be obtained from the results of experimental programs, such as uniaxial tensile tests (Abrishambaf *et al*. 2017, Graybeal and Baby 2013, Lampropoulos *et al*. 2016, Liu *et al*. 2016, Pyo *et al*. 2015, 2016, Rahdar and Ghalehnovi 2016, Singh *et al*. 2017, Tran *et al*. 2015, Wille *et al*. 2014, 2010), bending tests (Baby *et al*. 2012, Kanakubo 2006, Kang *et al*. 2010, López *et al*. 2015b, Mahmud *et al*. 2013, Singh *et al*. 2017, Wan *et al*. 2016, Yang *et al*. 2010, Yoo and Banthia 2015) and biaxial tests (Lee *et al*. 2017, Tysmans *et al*. 2015, Yoo *et al*. 2015). In order to study the effects of the fiber content on the tensile fracture properties of UHPFRC, Kang *et al*. (Kang *et al*. 2010) suggested a tri-linear tensile softening model obtained from a tensile fracture model of UHPFRC. They applied the inverse analysis method suggested by Uchida and Kurihara (1995) to determine the tensile fracture model. This method exploits the load-displacement curves obtained from flexural tensile tests to perform an inverse analysis using a finite element (FE) analysis and a poly-linear approximation method. Mahmud *et al*. (2013) studied the size effects on the flexural strength of similar notched UHPFRC beams by three-point bending tests. In this work, non-linear FE simulations were conducted using the concrete damage plasticity (CDP) model in ABAQUS and the material properties extracted from uniaxial tensile and compressive laboratory tests. To facilitate the numerical analysis and design more complex structures, Tysmans *et al*. (2015) adapt and validate the CDP model for both uni- and biaxial stress states, and for cement composites with large strain hardening capacity. In this case, an FE analysis in ABAQUS was performed. Pyo and El-Tawil (2015) proposed that the length of the tensile loading regime complicates the development of test setups that can capture the full tensile response at high strain rates. According to these authors, analytical and FEM were used to propose modifications to an existing test setup to enable it to conduct the accurate and practical testing of UHPFRC specimens in direct tension at a high strain rate. In this case, an isotropic elastic-plastic material model was used to model UHPFRC behavior in the LS-DYNA commercial FE program. Lampropoulos *et al*. (2016) studied the efficiency of using UHPFRC to strengthen existing reinforced concrete (RC) beams. In their work, dog bone-shaped specimens, tested under direct tensile loading, were used to develop a numerical model using FEM. In this case, UHPFRC behavior was modeled with elastic behavior up to the initiation of microcracking, followed by a second linear part into the strain hardening phase with multiple microcracking. Then after the macrocrack formation at ultimate resistance came the strain softening phase, which was modeled by a bi-linear model with the ATENA FE software. According to this work, the reliability of the numerical model was validated using the further experimental results of UHPFRC layers tested with flexural loading. In Yoo *et al*. (2017) a non-linear FE analysis was performed to simulate the flexural behaviors of UHPFRC beams. For this study, two different tension-softening curves obtained from a micromechanics-based analysis and an inverse analysis were incorporated. In this case, the discrete crack model, which is useful in situations in which the crack pattern can be predicted as a notched beam, was adopted to simulate the crack propagation at the assumed interface element in DIANA. Sadouki *et al*. (2017) modeled the structural response of RC cantilever beams retrofitted with a thin layer of UHPFRC. According to these authors, the complex cracking phenomenon of the resulting RC-UHPFRC composite system was carried out by a numerical model after incorporating the real non-linear materials laws to accurately predict mechanical behavior. In this case, a total strain rotating crack model based on a smeared crack approach was used to model constitutive UHPFRC behavior in DIANA. To validate the model, the experimental data obtained from an RC-UHPFRC cantilever were confronted with the numerical findings. Singh *et al*. (2017) investigated the efficacy of the hybrid approach to validate the existing concrete model to study the behavior of the large-scale structural members made up of UHPFRC. In this work, numerical models were developed and validated with the test results of the beams for which the CDP model was adopted to characterize the UHPFRC behavior in ABAQUS. Furthermore, the material parameters required to define the constitutive model were identified by conducting direct/uniaxial tension and compression tests. Guo *et al*. (2018) aimed to develop an adequate constitutive UHPFRC model for low-velocity impact simulations. In this case, current constitutive models of the concrete-like materials implemented into LS_DYNA were briefly overviewed.

A fracture mechanics non-linear hinge model has been developed and validated through experimental data by the authors to model UHPFRC behavior in a 4PBT (López *et al*. 2016). The main aim of this model is to provide a tool that makes the determination of a complete UHPFRC tensile constitutive relationship from a single test possible. An analytical formulation has been developed to describe non-linear hinge behavior. Moreover, a numerical model is developed in this paper to validate the non-linear hinge model (López *et al*. 2016) to derive the tensile UHPFRC's properties from the load-deflection response obtained from ThirdPBT experimental tests.

2. Non-linear hinge model proposed (López *et al*. 2016)

The complete load-displacement description at the mid-span UHPFRC behavior in a four-point bending test requires a non-linear fracture mechanics model because the discrete macrocrack formation phenomenon plays a very important role in this case. The model proposed herein can be applied only to a third-point bending test (ThirdPBT) setup, which is a specific type of four-point bending test according to the geometrical conditions in Fig. 1. It consists of a continuous crack model in which certain kinematic assumptions are made along a given length surrounding the crack (hinge length), inside which deformations are

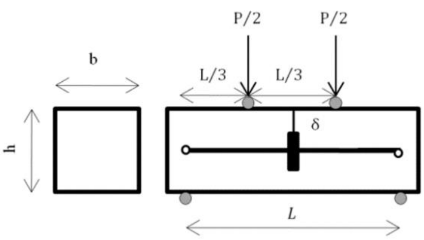

Fig. 1 The third-point bending test (ThirdPBT) setup

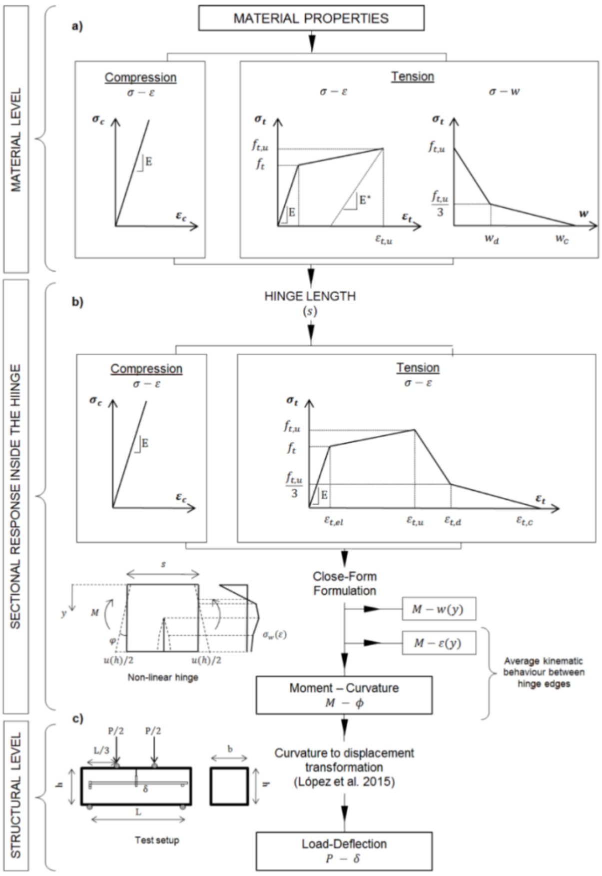

Fig. 2 Non-linear hinge model scheme

smeared. These assumptions mean that inside the hinge length, concrete behavior can be reduced to a single cross-section regardless of the real state of the stress surrounding the crack. A summary of the proposed non-linear hinge model is presented in Fig. 2 and is briefly described below.

2.1 Material level

The developed hinge model entails having to assume constitutive behavior in both tension and compression (Fig. 2(a)). As a reference, a bilinear stress-strain law along the ascending branch in tension is used. This part of the law is about the elastic and hardening response of UHPFRC. Once ultimate strength has been achieved, softening tensile behavior is described with a stress-crack opening relationship. The stress at the change of slope is set at one-third of ultimate tensile strength (see Fig. 2(a)). The constitutive law in compression is considered linear elastic at any strain. So the parameters that define constitutive

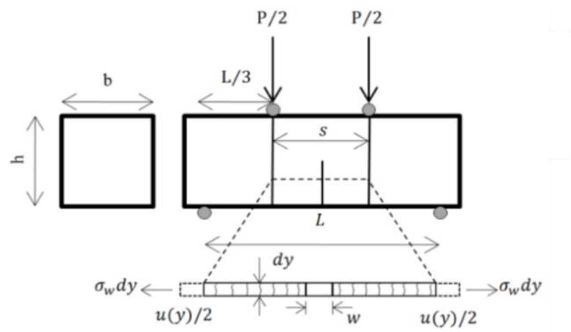

Fig. 3 Four-point bending test with a non-linear hinge (RILEM TC 162-TDF 2002)

UHPFRC behavior are: cracking strength (f_t), ultimate tensile strength ($f_{t,u}$) and its corresponding strain ($\varepsilon_{t,u}$), the crack opening at the change of slope (w_d), the crack opening at zero stress (w_c), the elastic modulus (E) and the unloading modulus (E^*).

2.2 Definition of the non-linear hinge

The proposed non-linear hinge model is based on Olesen's model (Olesen 2001), but includes different hypotheses to take into account the strain-hardening UHPFRC behavior according to Ostergaard *et al*. (2005). The proposed non-linear hinge scheme is shown in Fig. 3 for a ThirdPBT. The two variables in the test setup configuration in Fig. 3 are specimen depth (h) and span (L), which define the slenderness ratio ($\lambda = L/h$).

Once the stress at the most tensioned fiber reaches the peak tensile stress, a macrocrack appears with maximum tensile stress $f_{t,u}$ at the crack tip. To be able to apply the beam theory based on the Navier-Bernoulli hypothesis, the crack is smeared along the non-linear hinge length regardless of the real state of the stress inside this area. Therefore, the non-linear hinge model represents the average UHPFRC behavior inside the hinge length (s).

If the hypothesis of considering plane strain deformation inside the non-linear hinge is assumed, the sectional hinge response can be determined using a smeared stress-strain relationship within the hinge. Hence, it is possible to turn the softening stress-crack opening material relationship into a stress-strain relationship inside the non-linear hinge using (1) and (2). Fig. 2(b) depicts the constitutive - law used to describe the sectional response of the non-linear hinge, which is derived from the material's properties (Fig. 2(a)), along with the notation of the parameters used to model the UHPFRC sectional response within the non-linear hinge.

$$\varepsilon_{t,d} = \frac{w_d}{s} + \varepsilon_{t,u} - \frac{2f_{t,u}}{3E^*} \quad (1)$$

$$\varepsilon_{t,c} = \frac{w_c}{s} + \varepsilon_{t,u} - \frac{f_{t,u}}{E^*} \quad (2)$$

2.3 Closed-form formulation

By assuming the constitutive relationship in Fig. 4, and that the strain plane remains plane inside the hinge, the generalized forces (axial and bending forces) can be

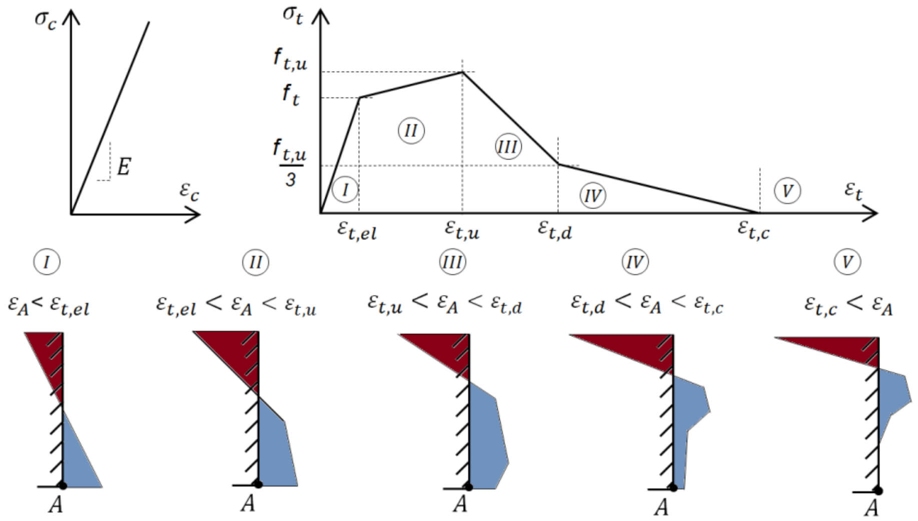

Fig. 4 Stress-strain relationship (above) for different stages (below)

obtained by integrating the compression and tension stress blocks. Following the steps pointed out in Soranakom *et al*. (Soranakom and Mobasher 2007), the axial and flexural capacity of the non-linear hinge can be expressed according to two parameters: the average curvature (ϕ) and the strain at the most tensioned fiber (ε_t).

As the stress-strain relationship defined in Fig. 4 is a quadrilinear curve, five different integration scenarios can be found depending on the strain reached at the most tensioned fiber according to Fig. 4: (Stage I) linear elastic up to the matrix-cracking strain, $\varepsilon_{t,el}$; (Stage II) strain-hardening behavior characterized by multiple microcracking up to crack localization, $\varepsilon_{t,u}$; (Stages III and IV) softening behavior characterized by macrocrack development up to the strain at zero stress, $\varepsilon_{t,c}$; (Stage V) fiber debonding. From the axial force equilibrium, ϕ -ε_t can be derived. Once this relationship has been established, the bending moment equation can be used to determine the M-ϕ relationship (see Table 3 in López *et al*. 2016).

2.4 Average curvature to displacement at the mid-span in a 4PBT

Non-linear hinge models are usually accompanied by a simplified formulation to determine the displacement according to any of the kinematic parameters of the hinge. The most widely used kinematic parameter for this purpose is the average curvature inside the hinge, which is the parameter employed by the authors.

The deflection to curvature transformation method developed herein focused on a ThirdPBT, and its extension to other 4PBTs should be checked. The relationship is established by Timoshenko Eq. (3). By considering non-linear curvature distribution, the non-linearity in bending is taken into account.

$$\delta = \frac{L}{2}\int_0^{L/2} \phi(x)dx - \int_0^{L/2} \phi(x)\left[\frac{L}{2} - x\right]dx + \frac{1}{GA_Q}\int_0^{L/2} Q(x)dx \quad (3)$$

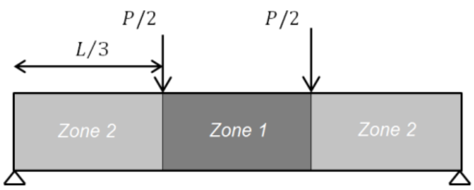

Fig. 5 Zones in the ThirdPBT

The integration of (3) requires a curvature distribution hypothesis along the beam in accordance with the applied load. Even though the theoretical M-ϕ relationship was obtained in Section 2.3, inverse relation ϕ-M is very difficult to obtain, and analytically integrating the resulting equations to obtain the ϕ-δ relationship can be very complicated. For this reason, it is necessary to assume a $\phi(x)$ distribution, which has to be easily integrated and must approach the theoretical relationship. For this purpose, in Zone 2 (see Fig. 5) the deflection at the mid-span to curvature transformation assumes a linear elastic distribution of the curvature up to approximately 70% of the maximum load, a logarithm hypothesis from this point on, even in the unloading branch, and a constant one in Zone 1 (see Fig. 5).

In accordance with the above-described assumptions, the method developed by the authors in López *et al*. (2015a) is used as it allows the deflection at the mid-span to be determined from the average curvature values at the central one-third in a 4PBT using a simple Eq. (4), and vice versa (5).

$$\delta = \min\begin{pmatrix} \frac{23L^2}{216}\emptyset + \frac{12P}{25Eb}\left(\frac{L}{h}\right) \\ \frac{5L^2}{72}\emptyset + \frac{P}{6Eb}\left(\frac{L}{h}\right)^3 + \frac{12P}{25Eb}\left(\frac{L}{h}\right) \end{pmatrix} \quad (4)$$

$$\emptyset = \max\begin{pmatrix} \frac{216}{23L^2}\left[\delta - \frac{12P}{25Eb}\left(\frac{L}{h}\right)\right] \\ \frac{72}{5L^2}\left[\delta - \frac{P}{6Eb}\left(\frac{L}{h}\right)^3 - \frac{12P}{25Eb}\left(\frac{L}{h}\right)\right] \end{pmatrix} \quad (5)$$

Before crack localization, the average curvature is the same as the curvature at each point inside Zone 1. However,

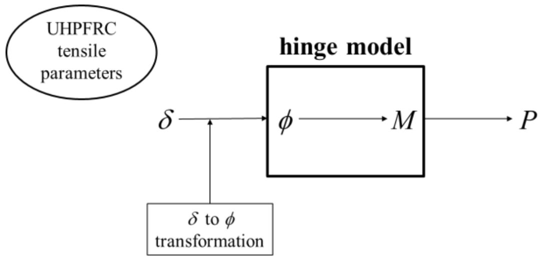

Fig. 6 State determination

after crack localization has taken place, the non-linear hinge model enables the consideration of an average curvature inside the non-linear hinge. If the considered hinge length is L/3, the curvature distribution in Zone 1 can be taken as being constant. According to this assumption, the disturbed cracked section is considered to be smeared over Zone 1.

2.5 State determination of the model

The state determination of the proposed closed-form non-linear hinge model can be schematically described as follows: the constitutive tensile parameters of UHPFRC are set and the displacement at the mid-span or deflexion (δ) is established as initial input. Then the transformation that relates δ to the average curvature (ϕ) is used (5). The hinge model is applied, and the bending moment (M) is obtained as a result. The numerical value of the applied load (P) can be obtained from M. Fig. 6 outlines the process of the above-described state determination.

3. Numerical finite element modeling

Crack formation and propagation can be a very important non-linear process in concrete structures. Nowadays, FE-codes based on non-linear material models are capable of very accurately predicting the mechanical behavior of concrete structures subjected to loads with different grades of complexity. With the evolution of new materials such as UHPFRC, it is necessary to both review and adapt concrete material models (Tysmans *et al*. 2015).

Two different approaches are frequently used in FE-codes for computational simulations of crack propagation in RC structures: the Discrete and Smeared Crack Approaches (Rots 2002, Rots and Blaauwendraad 1989). The Discrete Crack Approach models a crack as a geometrical discontinuity. Such models are used mainly in structures in which the crack path is known beforehand (Sadouki *et al*. 2017). In the Smeared Crack Approach, cracks are assumed to be smeared over continuum finite elements and no predefined position of cracks is needed. A cracked material is then treated as a continuum, but with modified material properties to account for cracking (Sadouki *et al*. 2017).

In this work, numerical modeling is developed using the FE software DIANA (DIANA (Software) 2017).

3.1 Constitutive behavior

To model tensile UHPFRC constitutive behavior, two different approaches are used: a *Smeared Cracking Approach* and a *Discrete Cracking Approach*.

<u>*Smeared Cracking Approach:*</u>

In this approach the constitutive model for UHPFRC is based on a fixed total strain crack model expressed according to the crack opening curve. In this case, to model UHPFRC tensile behavior in DIANA FEA, the “fiber-reinforced concrete model (FRCCON)” from the Fédération Internationale du Béton/International Federation for Structural Concrete (fib) working groups is used as a constitutive model (DIANA (Software) 2017). The model can be specified according to either the total strain or the crack opening. These two functions are related with the crack bandwidth parameter (h). The crack-opening is transformed into a strain by normalizing the crack-opening (w) by the crack bandwidth (h).

The crack bandwidth used was obtained from the “Rots’ element-based method” implemented into DIANA FEA (DIANA (Software) 2017), in which h depends on the size, shape and interpolation function of the finite element used. In this way, the fracture is released over this width of the FE to obtain objective results as regards the mesh refinement (Rots 2002, Rots and Blaauwendraad 1989).

For linear two-dimensional elements (DIANA (Software) 2017)

$$h = \sqrt{2A} \tag{6}$$

For higher order two-dimensional elements (DIANA (Software) 2017)

$$h = \sqrt{A} \tag{7}$$

where A is the total area of the element.

<u>*Discrete Cracking Approach:*</u>

In this approach the constitutive model for UHPFRC is founded on the discrete cracking model as interface behavior. The constitutive law for discrete cracking in DIANA is based on a total deformation theory, which expresses tractions according to the total relative displacements, crack width and crack slip. In this case, to model UHPFRC constitutive tensile behavior in DIANA FEA, a multi-linear function relating the relative displacements Δu_n normal to the interface and the tensile tractions t_n normal to the interface is used (DIANA (Software) 2017).

This behavior is forced only on the central beam section (Fig. 7). To fulfil this objective tensile strength (f_t) and ultimate tensile strength ($f_{t,u}$) are reduced by 2%. The rest of the beam is modelled using the model described in the *Smeared Cracking Approach*.

To model compression UHPFRC constitutive behavior, the MC-1990 curve is used in both cases (DIANA (Software) 2017).

3.2 Finite element mesh

The ThirdPBT has been modeled with a 2D quadratic plane stress eight-node quadrilateral element (CQ16M) when the *Smeared* and *Discrete Cracking Approaches* are

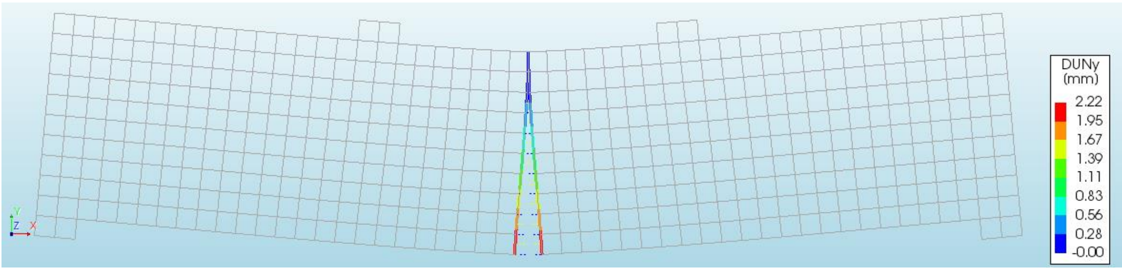

Fig. 7 Interface-relative displacements for the *Discrete Cracking Approach*

used. Besides, when the *Discrete Cracking Approach* is used, a quadratic 2D 3+3 nodes line interface element (CL12I) is placed on the central beam section. Fig. 7 shows the mesh used for the finite element model. A 10-mm element length was used for the model. Using this interface element, it was possible to model the discrete behavior of the crack at the mid-span cross-section (Fig. 7). The load was applied to the steel load plates by gradual increasing displacement.

3.3 Analysis procedure

A non-linear analysis was carried out by an *incremental-iterative* solution procedure.

For the load steps application (the *incremental* part), an adaptive loading iteration-based method was used. The size of increments was limited by the convergence characteristics of the selected iteration process. The allowable step size depends on the amount of the non-linearity in the increment, which is used in combination with the Arc-length method.

For the *iterative* part, the Modified Newton-Raphson method was carried out because, in situations where Regular Newton-Raphson does not converge any more, the Modified Newton-Raphson process can sometimes still converge. Moreover, a Line Search algorithm is also used because, in structures with strong nonlinearities, for instance cracking, Line Search algorithms can increase the convergence rate and are especially useful if the ordinary iteration process fails. To check the convergence of the iteration process, the energy norm was used.

The theoretical formulation of the model, the adopted numerical procedures and the employed solution strategy are described in detail in DIANA user's manuals (DIANA (Software) 2017).

4. Experimental validation

The experimental validation of the non-linear hinge requires the definition of an inverse analysis method to determine the constitutive material properties that derive from the bending test. As the non-linear hinge model requires a constitutive relationship in tension, which is *a priori* unknown, the iterative inverse analysis (I-IA) described in (López *et al*. 2015a) was used to determine it (see Fig. 8). An experimental program was run to validate the non-linear hinge model and the inverse analysis procedure by comparing the experimental measurements on

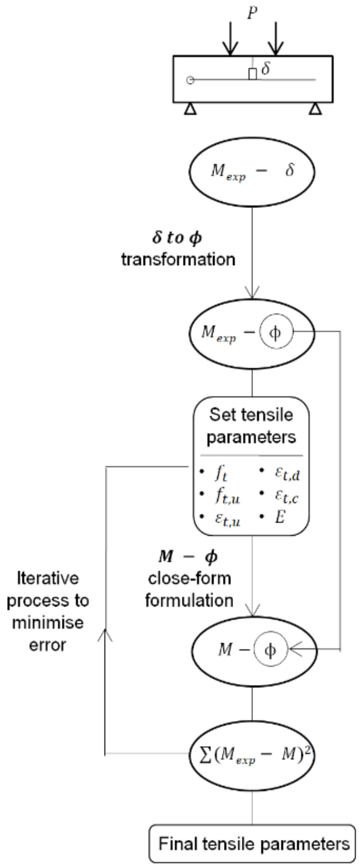

Fig. 8 Scheme of the iterative load-curvature inverse analysis method (I-IA) (López *et al*. 2015a)

the boundaries of the central one-third to the expected sectional response offered by the non-linear hinge model, which was obtained from the constitutive behavior that derived from the inverse analysis method. Besides, the material parameters obtained from the I-IA were used as input in the numerical FEM and the results were compared to the experimental results in order to numerically validate the hinge model.

It is common to use either the equivalent flexural strength, σ_{fl}, instead of the applied load, *P*, or the moment at the mid-span, *M*. The used transformations are shown in (8) for a rectangular cross-section and a ThirdPBT setup. When using (8), the bending moment can be converted into equivalent flexural stress, and the experimental and numerical values of σ_{fl} can be compared for each value.

$$\sigma_{fl} = \frac{6M}{bh^2} = \frac{PL}{bh^2} \tag{8}$$

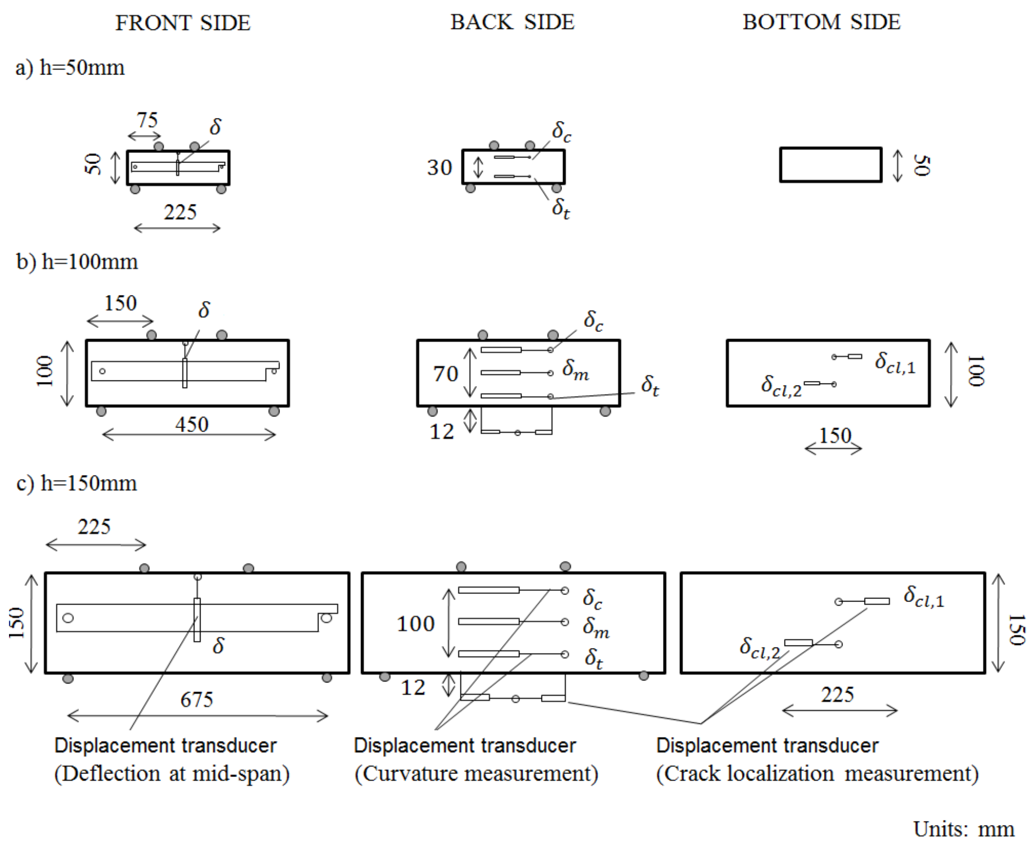

Fig. 9 Specimen geometries and location of the used displacement transducers (López *et al*. 2015b)

4.1 Experimental program

For the purpose of validating the non-linear hinge model and the proposed inverse analysis method, the experimental program developed in (López *et al*. 2015b) was used.

In this experimental program three different types of square cross-section specimens were prepared with a variable depth of 50, 100 and 150 mm. The *L/h* ratio was constant and equaled 4.5 for them all. A 2% volume of the smooth-straight (13/0.20) steel fibers was used in an Ultra-High-Performance cementitious matrix with an average compressive strength of 169.9 MPa. Eight 50- and 100-mm specimens, and four 150-mm specimens, were made. The geometry of the specimens and the ThirdPBT setup are shown in Fig. 9. In 25% of the tested specimen, the macrocrack appeared out of the central one-third. Those cases in which the macrocrack appeared out of the central one-third were not considered.

According to Fig. 9, a displacement transducer was used to record the displacement at the mid-span on the front side. Three displacement transducers were used on the rear side of the 100- and 150-mm specimens to obtain the experimental average curvature inside the central one-third. With the 50-mm deep specimens, the shallower depth forced having to use only two displacement transducers. On the bottom side, two staggered extensometers were employed at a distance of 12 mm from the specimen's tensile face. The setup configuration for the 50-mm deep specimens made it impossible to place these displacement transducers.

Table 1 The constitutive relationships obtained from I-IA

Specimen		E (GPa)	f_t (MPa)	$f_{t,u}$ (MPa)	$\varepsilon_{t,u}$ ‰	$f_{t,d}$ (MPa)	$\varepsilon_{t,d}$ ‰	$\varepsilon_{t,c}$ ‰	w_d (mm)	w_c (mm)
Iterative Inverse Analysis, 50-mm	1	46	10.58	11.44	1.8	3.81	13.5	83.4	0.94	6.21
	2	47	10.55	11.45	3.2	3.82	20.4	75.0	1.35	5.48
	3	48	12.13	12.68	2.5	4.23	19.0	106.9	1.31	7.93
	4	49	13.84	14.15	3.2	4.72	16.5	75.7	1.07	5.55
	5	48	13.34	13.48	5.8	4.49	17.7	81.5	0.97	5.79
	6	46	9.39	13.33	3.7	4.44	19.6	85.7	1.26	6.26
100-mm	1	49	9.96	12.80	3.9	4.27	9.7	35.5	1.00	4.95
	2	54	9.96	12.54	4.4	4.18	13.4	39.2	1.49	5.44
	3	54	10.61	11.86	5.5	3.95	16.2	39.8	1.75	5.35
	4	48	9,96	12.62	3.4	4.21	10.6	31.1	1.21	4.37
	5	48	11.81	15.47	5.1	5.16	12.6	33.6	1.30	4.53
	6	47	9.47	11.62	2.7	3.87	11.5	31.9	1.45	4.58
150-mm	1	49	9.96	14.13	4.3	4.71	13.8	24.6	2.37	4.93
	2	49	9.22	12.85	4.2	4.28	12.4	27.3	2.06	5.51
	3	49	10.20	13.67	5.3	4.56	14.8	27.0	2.38	5.23

The constitutive parameters obtained after applying the I-IA using the closed-form are shown in Table 1.

4.2 Numerical model application

The material properties of I-IA using the non-linear hinge model closed-form shown in Table 1 were implemented into the numerical model described in Section 3 and compared to the experimental program results.

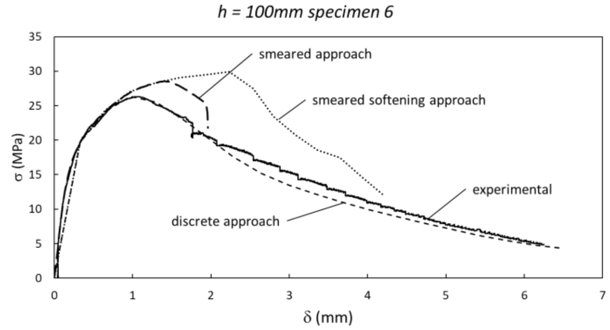

Fig. 10 Equivalent bending stress-displacement at the mid-span curves

Fig. 10 shows the results obtained when the constitutive parameters resulting from I-IA by using the non-linear hinge model for specimen number 6 with h=100 mm were implemented into the numerical model in both cases: the *Smeared Cracking Approach* and the *Discrete Cracking Approach*.

The *Smeared Approach* is represented in two responses depending on the value of the imposed displacement at the load plates (Fig. 10): a *Smeared Approach* focused on the ascending branch of the response, obtained by imposing a low displacement value, and a *Smeared Softening Approach* in an attempt to develop a complete curve response, obtained by imposing a higher displacement value. As seen in Fig. 10, the *Smeared Approach* of the numerical model does not accurately fit the experimental curve, that is, the *Smeared Approach* seems to accumulate more fracture energy. Moreover, if attention is paid to the two smeared curves, we can see that they do not represent the same σ_{tu} value nor the same initial stiffness. The reason for this could be that the crack bandwidth used, obtained from the "Rots' element-based method" implemented into DIANA FEA (DIANA (Software) 2017) for the "fiber-reinforced concrete model (FRCCON)" does not avoid the model mesh size dependence. The adaptation of this model, which works well with plain and conventional fiber-reinforced concrete, is not reliable enough when implemented into materials with significant bulk energy dissipation, such as UHPFRC. A possibility of improving the smeared approach response could be to use fracture-softening models for the Smeared Crack Approach available in Diana DIANA FEA (DIANA (Software) 2017) and by scaling the stress-strain constitutive law to guarantee fracture energy preservation (Jirásek 2017, Sadouki *et al*. 2017, Switek 2008). If the *Discrete Approach* curve of the model is considered, excellent accuracy is achieved compared to the experimental one. For these reasons, the *Discrete Approach* seems suitable for modeling tensile UHPFRC behavior in a

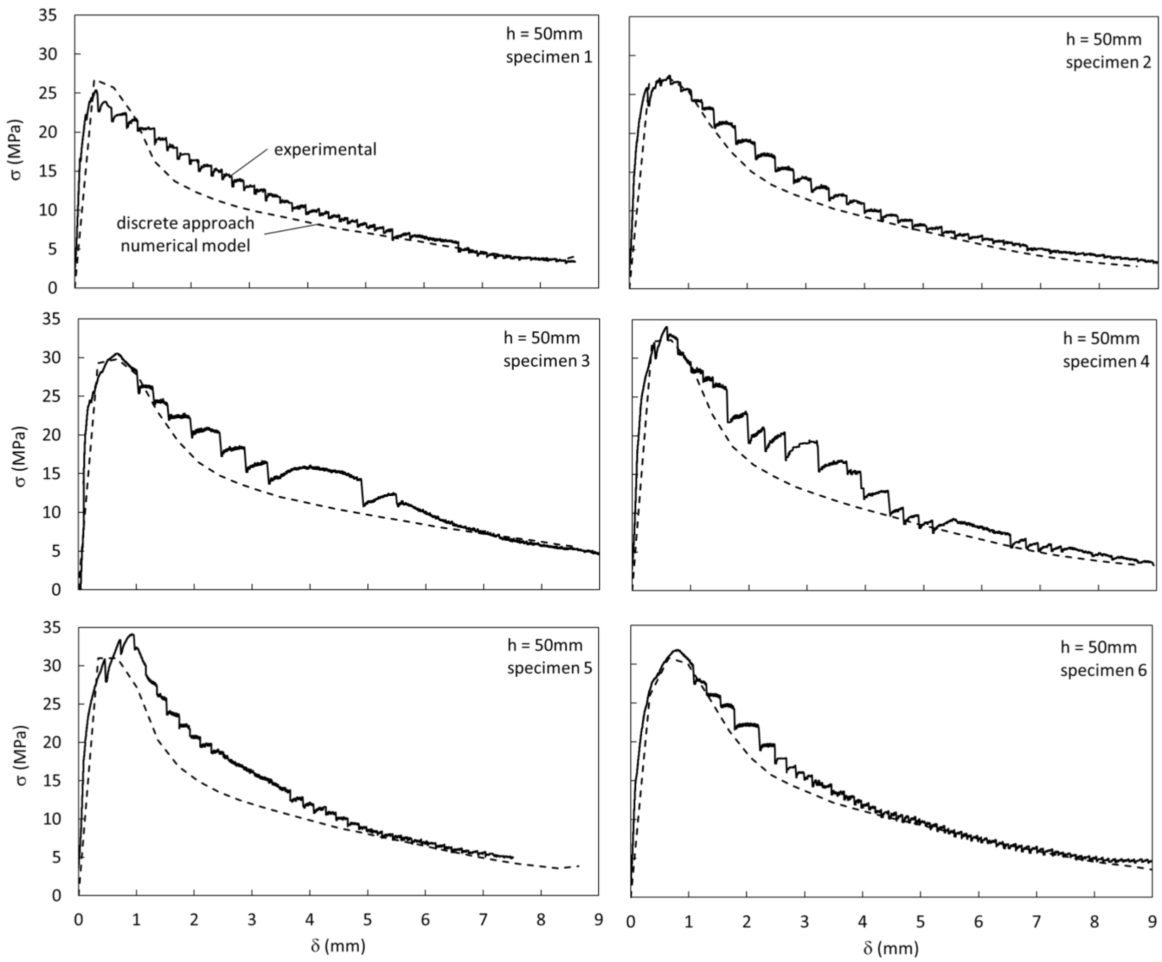

Fig. 11 Equivalent bending stress-displacement at the mid-span curves for the h=50 mm specimens

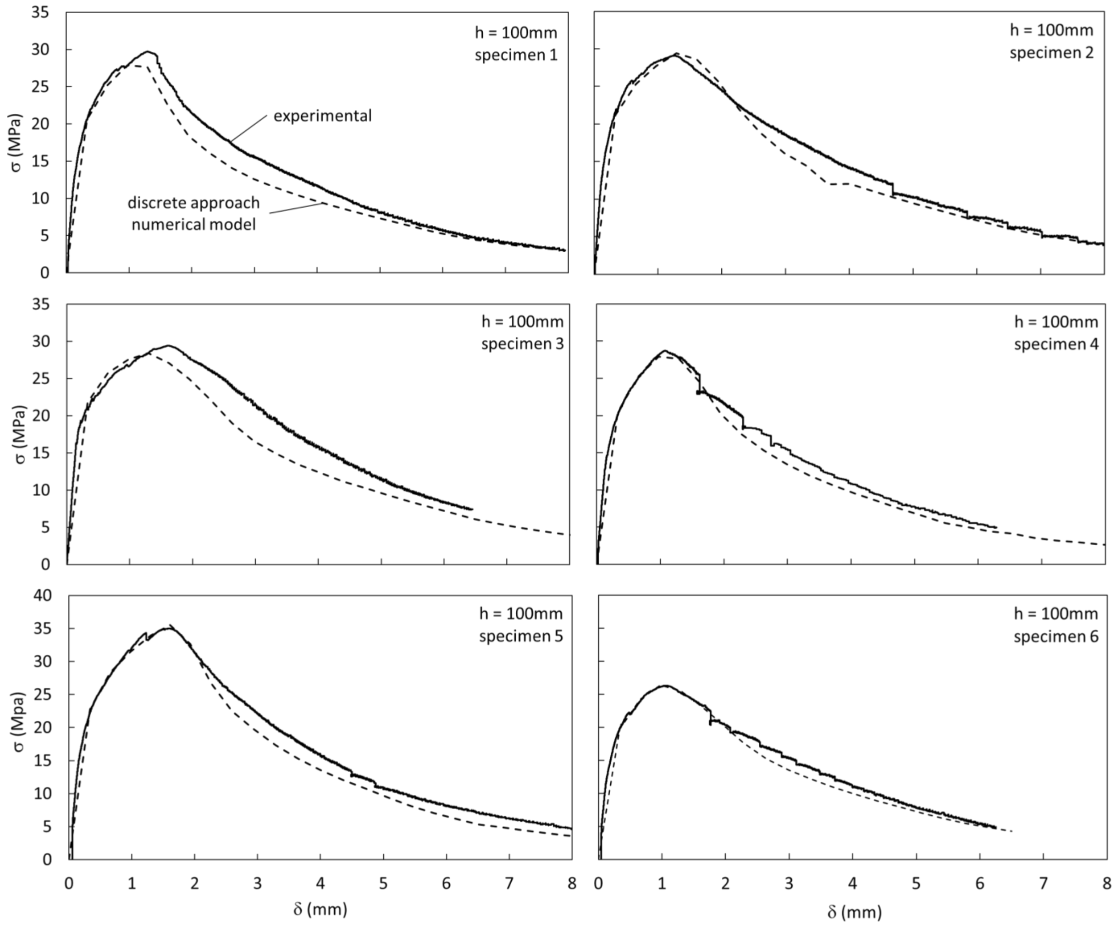

Fig. 12 Equivalent bending stress-displacement at the mid-span curves for the *h*=100 mm specimens

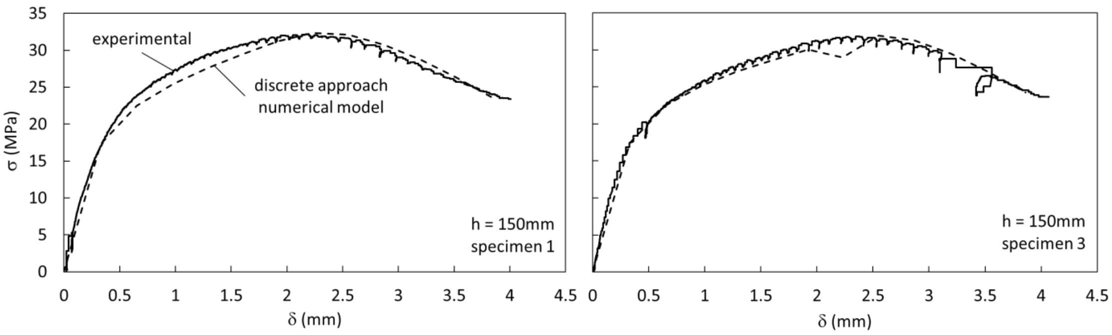

Fig. 13 Equivalent bending stress-displacement at the mid-span curves for the *h*=150 mm specimens

ThirdPBT. This assumption is coherent with the experimental response because it represents the high concentration of the stresses and strains generated in a specific section.

In Fig. 11, Fig. 12 and Fig. 13 the experimental stress-displacement at the mid-span curves and the numerical model with the *Discrete Approach* are compared for the specimens considered in the experimental program.

We can see that the numerical model using the *Discrete Approach* seems to fit the experimental behavior. So it can be concluded that the numerical model with the *Discrete Approach* is reliable enough and, therefore, the closed-form non-linear hinge model is a suitable method to derive the tensile UHPFRC's properties from the load-deflection response obtained from the ThirdPBT experimental tests. However, some numerical curves did not completely fit the experimental ones in terms of f_{tu} (for example, see *h*=50 mm, specimen 5 in Fig. 11). The reason for this inaccuracy might be due to an *incremental-iterative* process carried out in the analysis procedure of the numerical model. To improve this fitting, a particular treatment was developed in the analysis procedure of the numerical model. This improvement consists in developing an Analysis Continuation Approach (see Section 4.3 below).

4.3 Analysis continuation approach

There are some situations in which non-linear analysis

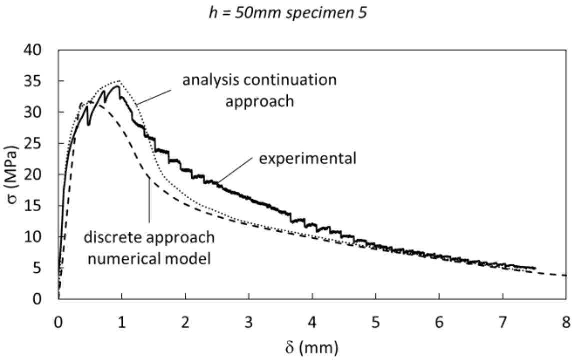

Fig. 14 Equivalent bending stress-displacement at the mid-span curves for the h=50 mm specimen 5

solutions may be hard to obtain for all the steps using only one single incremental-iterative solution procedure. For this reason, it is better to split the load incrementation process into more than one part so that different solution methods can be applied. The DIANA software offers this possibility. The new analysis that follows the preceding one starts using the last converged results obtained from the previous one. Each analyzed specimen has its particular analysis process. That is, the analysis process used for one specimen is not general for the others because each specimen has converged in its own particular way.

By way of example, Fig. 14 shows improved accuracy with the Analysis Continuation Approach applied for the h=50 mm specimen 5.

4.4 Equivalent bending strength versus curvature

The equivalent bending strength (σ_{fl}) *versus* curvature on the boundaries of the non-linear hinge (ϕ) relationship was obtained from two different sources: (i) the experimental data from the displacement transducer on the rare side of the specimen (see Fig. 9); (ii) using the stress-strain sectional behavior law that derives from I-IA and the non-linear hinge model.

In case (i), the experimental curvature was obtained by the linear regression of the strain measurements of three displacement transducers, δ_c, δ_m, and δ_t (see Fig. 9), placed on the rare side of the 100-mm and 150-mm specimens. The experimental curvature in the 50-mm specimens was obtained following (9), where d_ϕ is the distance between the displacement transducer, and s is gage length or hinge length.

$$\phi_{50mm} = \frac{|\delta_t - \delta_c|/s}{d_\phi} \tag{9}$$

The I-IA results, obtained by using the closed-form non-linear hinge model shown in Table 1, were implemented into the *Discrete Approach* numerical model. The σ_{fl}-ϕ curve from the numerical model can be obtained following the displacements of the finite element nodes situated in the same position of the displacement transducers.

Fig. 15 shows the three different σ_{fl} *versus* the normalized average curvature (ϕ_n=ϕh) obtained for three different specimens from the three different specimen depths used: h=50 mm, h=100 mm and h=150 mm. Both, the experimental and I-IA hinge model curves were compared to the one of the *Discrete Approach* numerical model.

The *Discrete Approach* numerical model accurately represents the equivalent bending strength *versus* the normalized average curvature, as shown in Fig. 15. It proves that the non-linear hinge model is reliable enough.

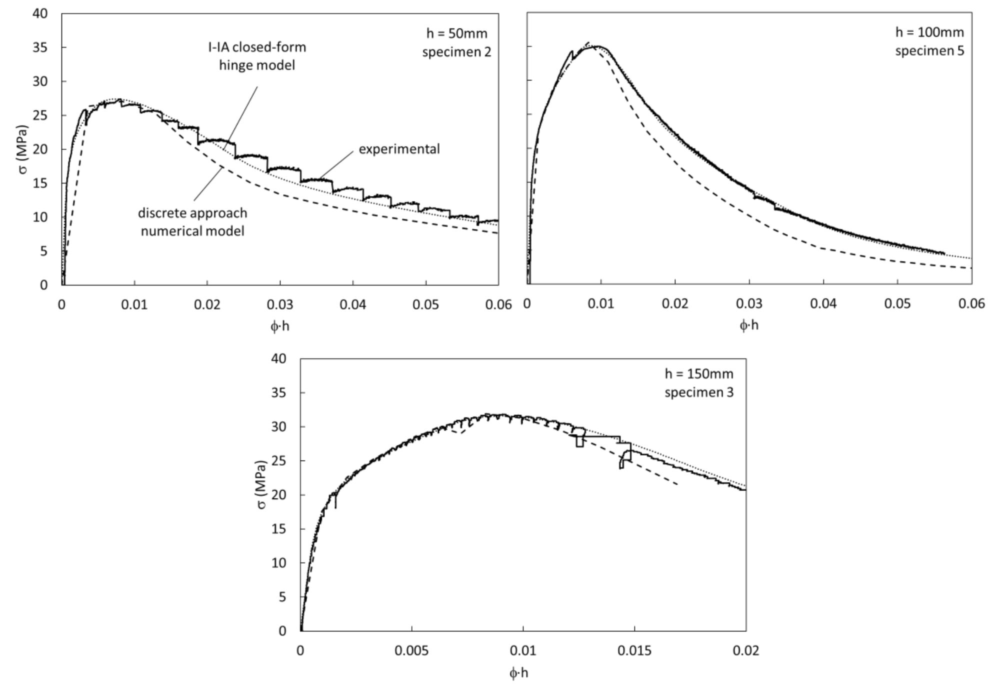

Fig. 15 Equivalent bending strength (σ_{fl}) *versus* normalized average curvature ($\phi{\cdot}h$) for the h=50 mm specimen 2, the h=100 mm specimen 5 and the h=150 mm specimen 3

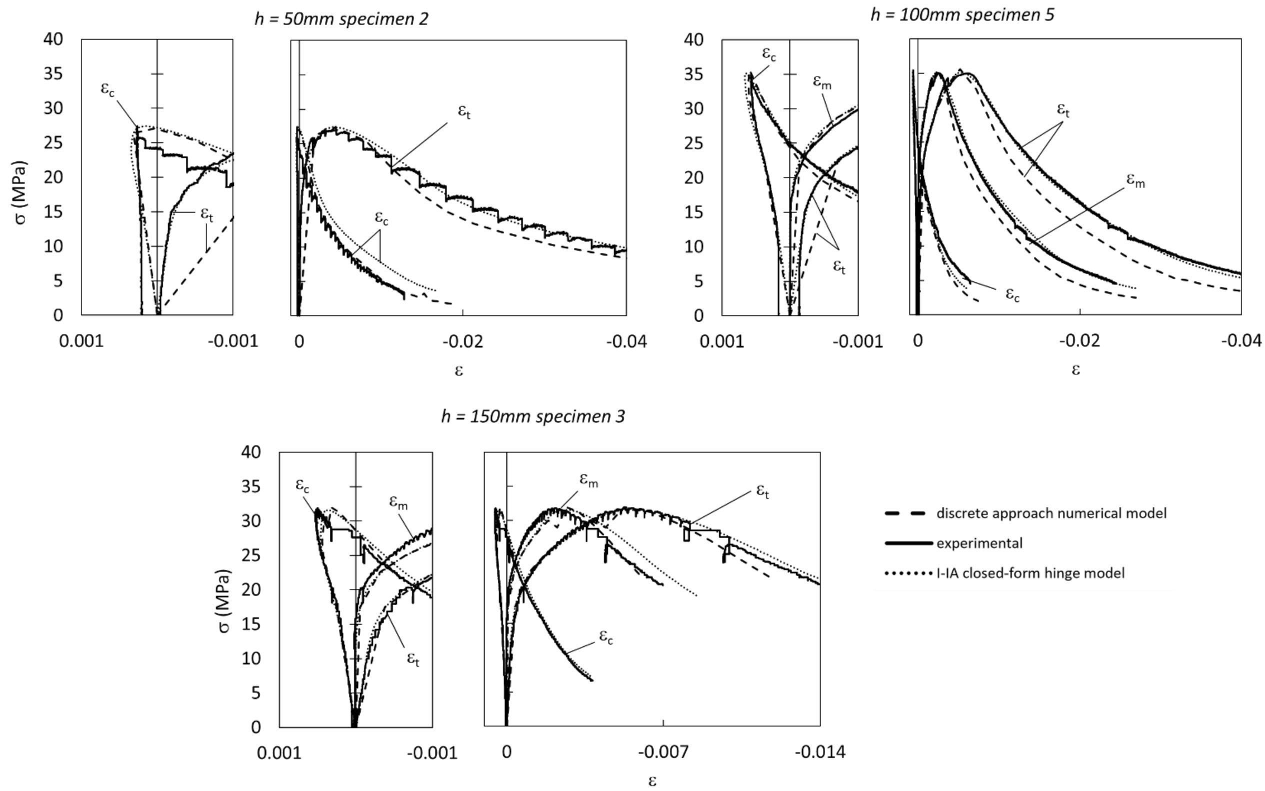

Fig. 16 Equivalent bending strength (σ_{fl}) *versus* the average strain at different depth positions (ε_c, ε_m, and ε_t) for the *h*=50 mm specimen 2, the *h*=100 mm specimen 5 and the *h*=150 specimen 3

4.5 Average strain profile inside the hinge

Experimental equivalent flexural strength *versus* the average strain on the non-linear hinge on the different depth position curves was obtained using the displacement transducers placed on the back and bottom sides of the tested specimens (see Fig. 9). The average strain values ε_c, ε_m, and ε_t, represented in Fig. 16 were obtained by dividing the δ_c, δ_m, and δ_t displacement transducer measurements by their gage length, which corresponded to the constant bending moment area.

The average strain values at the different depth positions obtained from the experimental tests were compared to the values that derived from the constitutive law obtained by I-IA.

The I-IA results, obtained from using the closed-form non-linear hinge model shown in Table 1, were implemented into the *Discrete Approach* numerical model. The equivalent bending moment *versus* the average strain at the different depth positions curve from the numerical model can be obtained following the displacements of the finite element nodes situated in the same position of the displacement transducers.

Figure 16 shows the equivalent flexural strength (σ_{fl}) *versus* the average strain at different depth positions curves (ε_c, ε_m, and ε_t) obtained for three different specimens from the three different specimen depths used: h=50 mm, h=100 mm and h=150 mm. Both the experimental and I-IA hinge model curves were compared to the one of the *Discrete Approach* numerical model.

The *Discrete Approach* numerical model accurately represents the equivalent bending strength *versus* the average strain at the different depth positions, as seen in Fig. 16. The two models offer similar results and fit the experimental results. Both are valid to determine the tensile properties of UHPFRC in a ThirdPBT.

5. Conclusions

A non-linear Finite Element Model to validate a closed-form non-linear hinge model to determine the load-deflection response of UHPFRC in ThirdPBTs was presented in this paper.

- The closed form non-linear hinge model was validated by resorting to robust non-linear finite element modeling and a set of fifteen ThirdPBTs with a variable depth and constant slenderness ratio of 4.5.
- The *Discrete Cracking Approach* of the numerical model was more adequate to model tensile UHPFRC behavior in a ThirdPBT.
- When using the tensile parameters that resulted from an iterative inverse analysis method using the presented closed-form non-linear hinge model, the *Discrete Cracking Approach* accurately describes: (a) the load deflection response; (b) the average bending curvatures; (c) the average longitudinal strains measured in the constant bending moment zone.
- As a result, inverse analysis methodologies based on the proposed closed-form non-linear hinge model can be

recommended to derive UHPFRC's tensile properties in ThirdPBTs.

Acknowledgments

This work forms part of Project "BIA2016-78460-C3-1-R" supported by the State Research Agency of Spain

References

Abrishambaf, A., Pimentel, M. and Nunes, S. (2017). "Influence of fibre orientation on the tensile behaviour of ultra-high performance fibre reinforced cementitious composites", *Cement Concrete Res.*, **97**, 28-40.

Baby, F., Graybeal, B., Marchand, P. and Toutlemonde, F. (2012). "Proposed flexural test method and associated inverse analysis for ultra-high-performance fiber-reinforced concrete", *ACI Mater. J.*, **109**(5), 545-555.

Baby, F., Graybeal, B., Marchand, P. and Toutlemonde, F. (2013). "UHPFRC tensile behavior characterization: Inverse analysis of four-point bending test results", *Mater. Struct., Mater. Constr.*, **46**(8), 1337-1354.

Casanova, P. and Rossi, P. (1996). "Analysis of metallic fibre-reinforced concrete beams submitted to bending", *Mater. Struct.*, **29**(6), 354-361.

DIANA (Software). (2017). "User's Manual- Release 10.2", *TNO DIANA, The Netherlands*, https://dianafea.com/manuals/d102/Diana.html.

Graybeal, B. and Baby, F. (2013). "Development of direct tension test method for ultra-high-performance fiber-reinforced concrete", *ACI Mater. J.*, **110**(110), 177-186.

Grtiger, J., Tue, N.V. and Wille, K. (2012). "Bending Behaviour and Variation of Flexural Parameters of UHPFRC", *3rd International Symposium on UHPC and Nanotechnology for High Performance Construction Materials,* Kassel University Press GmbH, 419-426.

Guo, W., Fan, W., Shao, X., Shen, D. and Chen, B. (2018). "Constitutive model of ultra-high-performance fiber-reinforced concrete for low-velocity impact simulations", *Compos. Struct.*, **185**, 307-326.

Jirásek, M. (2017). "Modeling of localized inelastic deformation", Short Course Given by Prof. M. Jirásek at Czech Technical University, 18-22/09/2017, Prague, September, 0-373.

Kanakubo, T. (2006). "Tensile characteristics evaluation method for ductile fiber-reinforced cementitious composites", *J. Adv. Concrete Technol.*, **4**(1), 3-17.

Kang, S.T., Lee, Y., Park, Y.D. and Kim, J.K. (2010). "Tensile fracture properties of an Ultra High Performance Fiber Reinforced Concrete (UHPFRC) with steel fiber", *Compos. Struct.*, **92**(1), 61-71.

Lampropoulos, A.P., Paschalis, S.A., Tsioulou, O.T. and Dritsos, S.E. (2016). "Strengthening of reinforced concrete beams using ultra high performance fibre reinforced concrete (UHPFRC)", *Eng. Struct.*, **106**, 370-384.

Lee, J.H., Hong, S.G., Joh, C., Kwahk, I. and Lee, J.W. (2017). "Biaxial tension-compression strength behaviour of UHPFRC in-plane elements", *Mater. Struct., Mater. Constr.*, **50**(1), 20.

Liu, J., Han, F., Cui, G., Zhang, Q., Lv, J., Zhang, L. and Yang, Z. (2016). "Combined effect of coarse aggregate and fiber on tensile behavior of ultra-high performance concrete", *Constr. Build. Mater.*, **121**, 310-318.

López, J.Á. (2017). "Characterisation of the tensile behaviour OF UHPFRC by means of four-point bending tests", Universitat Politècnica de València, Valencia, Spain.

López, J.Á., Serna, P., Navarro-Gregori, J. and Camacho, E. (2015a). "An inverse analysis method based on deflection to curvature transformation to determine the tensile properties of UHPFRC", *Mater. Struct.*, **48**(11), 3703-3718.

López, J.Á., Serna, P., Navarro-Gregori, J. and Coll, H. (2016). "A simplified five-point inverse analysis method to determine the tensile properties of UHPFRC from unnotched four-point bending tests", *Compos. Part B: Eng.*, **91**, 189-204.

López, J., Serna, P., Navarro-Gregori, J. and Coll, H. (2015b). "Comparison between an inverse analysis procedure results and experimental measurements obtained from UHPFRC Four-Point Bending Tests", *Seventh International RILEM Conference on High Performance Fiber Reinforced Cement Composites (HPFRCC7)*, H.G. H.W. Reinhardt, G.J. Parra-Montesinos, ed., RILEM Publications SARL, 185-192.

Maalej, M. and Li, V.C. (1994). "Flexural strength of fiber cementitious composites", *ASCE J. Mater. Civil Eng.*, ASCE, **6**(3), 390-406.

Mahmud, G.H., Yang, Z. and Hassan, A.M.T. (2013). "Experimental and numerical studies of size effects of Ultra High Performance Steel Fibre Reinforced Concrete (UHPFRC) beams", *Constr. Build. Mater.*, **48**, 1027-1034.

Olesen, J.F. (2001). "Fictitious crack propagation in fiber-reinforced concrete beams", *J. Eng. Mech.*, **127**(3), 272-280.

Ostergaard, L., Walter, R. and Olesen, J.F. (2005). "Method for determination of tensile properties of engineered cementitious composites (ECC)", *Construction Materials: Proceedings of ConMat'05 and Mindess Symposium*, 74.

Pedersen, C. (1996). "New production process, materials and calculation tecniques for fiber reinforced concrete pipes", PhD Thesis, Department of Structural Engineering and Materials.

Pyo, S. and El-Tawil, S. (2015). "Capturing the strain hardening and softening responses of cementitious composites subjected to impact loading", *Constr. Build. Mater.*, **81**, 276-283.

Pyo, S., El-Tawil, S. and Naaman, A.E. (2016). "Direct tensile behavior of ultra high performance fiber reinforced concrete (UHP-FRC) at high strain rates", *Cement Concrete Res.*, **88**, 144-156.

Pyo, S., Wille, K., El-Tawil, S. and Naaman, A.E. (2015). "Strain rate dependent properties of ultra high performance fiber reinforced concrete (UHP-FRC) under tension", *Cement Concrete Compos.*, **56**, 15-24.

Qian, S. and Li, V.C. (2007). "Simplified inverse method for determining the tensile strain capacity of strain hardening cementitious composites", *J. Adv. Concrete Technol.*, **5**(2), 235-246.

Rahdar, H. and Ghalehnovi, M. (2016). "Post-cracking behavior of UHPC on the concrete members reinforced by steel rebar", *Comput. Concrete*, **18**(1), 139-154.

Rigaud, S., Chanvillard, G. and Chen, J. (2012). "Characterization of bending and tensile behavior of ultra-high performance concrete containing glass fibers", *High Performance Fiber Reinforced Cement Composites 6: HPFRCC 6*, Eds. G.J. Parra-Montesinos, H.W. Reinhardt and A.E. Naaman, Springer Netherlands, Dordrecht, 373-380.

RILEM TC 162-TDF. (2002). "Recommendations of RILEM TC 162-TDF: Test and design methods for steel fibre reinforced concrete Design of steel fibre reinforced concrete using the sigma-epsilon method: principles and applications", *Mater. Struct.*, RILEM, **35**(249), 262-278.

Rots, J.G. (2002). "Comparative study of crack models", *Proceedings of the 3rd DIANA World Conference, Finite Elements in Civil Engineering Applications*, 17-28.

Rots, J.G. and Blaauwendraad, J. (1989). "Crack models for concrete, discrete or smeared? Fixed, multi-directional or rotating?", *HERON*, **34**(1), Delft University of Technology.

Sadouki, H., Denarié, E. and Brühwiler, E. (2017). "Validation of a

FEA model of structural response of RC-cantilever beams strengthened with a (R-) UHPFRC layer", *Constr. Build. Mater.*, **140**, 100-108.
Singh, M., Sheikh, A.H., Mohamed Ali, M.S., Visintin, P. and Griffith, M.C. (2017), "Experimental and numerical study of the flexural behaviour of ultra-high performance fibre reinforced concrete beams", *Constr. Build. Mater.*, **138**, 12-25.
Soranakom, C. and Mobasher, B. (2007). "Closed-form moment-curvature expressions for homogenized fiber-reinforced concrete", *ACI Mater. J.*, **104**(4), 351-359.
Stang, H. and Olesen, J.F. (1998). "On the interpretation of bending tests on FRC-materials", *Fracture Mechanics of Concrete Structures*, AEDIFICATIO Publishers, D-79104 Freiburg, Germany.
Switek, A. (2008). "Smeared crack modelling of fracture in materials with significant bulk energy dissipation", *École Polytechnique Fédérale de Lausanne*, Lausanne, 0-14.
Tran, N.T., Tran, T.K. and Kim, D.J. (2015). "High rate response of ultra-high-performance fiber-reinforced concretes under direct tension", *Cement Concrete Res.*, **69**, 72-87.
Tysmans, T., Wozniak, M., Remy, O. and Vantomme, J. (2015). "Finite element modelling of the biaxial behaviour of high-performance fibre-reinforced cement composites (HPFRCC) using concrete damaged plasticity", *Finite Elem. Anal. Des.*, **100**, 47-53.
Uchida, Y. and Kurihara, N. (1995). "Determination of tension softening diagrams of various kinds of concrete by means of numerical analysis", *Fracture Mechanics of Concrete Structures - FraMcoS 2*, AEDIFICATIO Unterengstringin, 17-30.
Wan, L., Wendner, R., Liang, B. and Cusatis, G. (2016). "Analysis of the behavior of ultra high performance concrete at early age", *Cement Concrete Compos.*, **74**(15), 120-135.
Wille, K., El-Tawil, S. and Naaman, A.E. (2014). "Properties of strain hardening ultra high performance fiber reinforced concrete (UHP-FRC) under direct tensile loading", *Cement Concrete Compos.*, **48**, 53-66.
Wille, K., Kim, D.J. and Naaman, A.E. (2010). "Strain-hardening UHP-FRC with low fiber contents", *Mater. Struct.*, **44**(3), 583-598.
Yang, I.H., Joh, C. and Kim, B.S. (2010). "Structural behavior of ultra high performance concrete beams subjected to bending", *Eng. Struct.*, **32**(11), 3478-3487.
Yoo, D.Y. and Banthia, N. (2015). "Numerical simulation on structural behavior of UHPFRC beams with steel and GFRP bars", *Comput. Concrete*, **16**(5), 759-774.
Yoo, D.Y., Kang, S.T., Banthia, N. and Yoon, Y.S. (2017). "Nonlinear finite element analysis of ultra-high-performance fiber-reinforced concrete beams", *Int. J. Damage Mech.*, **26**(5), 735-757.
Yoo, D.Y., Zi, G., Kang, S.T. and Yoon, Y.S. (2015). "Biaxial flexural behavior of ultra-high-performance fiber-reinforced concrete with different fiber lengths and placement methods", *Cement Concrete Compos.*, **63**, 51-66.

CC